SCIENCE CHINA
Technological Sciences

•Article•

May 2019 Vol.62 No.5: 839–848
https://doi.org/10.1007/s11431-018-9458-5

Analysis and evaluation of electromagnetic vibration and noise in permanent magnet synchronous motor with rotor step skewing

DONG QiChao[1], LIU XinTian[1*], QI HongZhong[2], SUN Chao[2] & WANG YanSong[1]

[1]*School of Mechanical and Automotive Engineering, Shanghai University of Engineering Science, Shanghai 201620, China;*
[2]*Guangzhou Automobile Group CO., LTD Automotive Engineering Institute, Guangzhou 511343, China*

Received August 27, 2018; accepted January 23, 2019; published online March 18, 2019

In this paper, a multi-physics simulation model capable of electromagnetic noise prediction is established, and the effectiveness of the established simulation model in predicting and evaluating electromagnetic noise is verified. Based on the verified motor model, a rotor step skewing model which can affect electromagnetic noise is proposed, and the influence of the skewing angle on electromagnetic noise is investigated in detail. By studying the spectral characteristics of the low-order radial magnetic force which has a great influence on electromagnetic noise, the distribution of electromagnetic noise characteristics of the permanent magnet synchronous motor (PMSM) with or without the rotor step skewing is compared and analyzed. Therefore, it lays a technological foundation for predicting and suppressing the electromagnetic vibration noise of electric vehicle (EV) driving motor in the electromagnetic design.

PMSM, electromagnetic noise, step skewing, multi-physics simulation model, spectrum analysis

Citation: Dong Q C, Liu X T, Qi H Z, et al. Analysis and evaluation of electromagnetic vibration and noise in permanent magnet synchronous motor with rotor step skewing. Sci China Tech Sci, 2019, 62: 839–848, https://doi.org/10.1007/s11431-018-9458-5

1 Introduction

The permanent magnet synchronous motor (PMSM) has apparent superiority as driving motor for an electric vehicle (EV) because of compact structure and high power density [1]. However, compared with the traditional car, the vehicle driven by motor has presented a new noise characteristic due to the change of the excitation source of vehicle noises [2]. In such a case, the sharply increase of high-frequency noises is particularly obvious. Moreover, some of these high-frequency noises distribute in the frequency range which is sensitive to human ears, thereby leading to a very uncomfortable feeling to drivers and passengers [3,4]. Therefore, investigating the noise characteristics of PMSM for vehicles is of great significance to reduce the noise and improve the sound quality of EVs [5,6].

Electromagnetic excitation is the root to electromagnetic noise. Specifically, the radial magnetic force mainly acts on the stator tooth surface, and presents the characteristics of space-time magnetic distribution in the air gap. The spatial order and deformable amplitude at different frequencies affect the electromagnetic noise distribution directly [7,8]. Meanwhile, the tangential magnetic force component produces the acting torque corresponding to the electromagnetic torque, which leads to the bending vibration of the tooth root, and then causing the torque ripple [9,10]. However, the tangential magnetic force component is the secondary factor of the electromagnetic noises [11].

At present, the studies in the noise characteristics of PMSM are mainly divided into two types. One is to analyze the distribution characteristics of electromagnetic noise from the excitation source, such as the harmonic modulation of current-time, magnetic control of air gap and space-time distribution of magnetic force. Another is that the causes of

* Corresponding author (email: xintianster@gmail.com)

some characteristic orders are studied to find a way to weaken the electromagnetic noise based on the result phenomenon of electromagnetic noise distribution. The former type mainly focuses on the distribution characteristics analysis of the magnetic harmonic components by controlling the current-time, and the analytical and numerical analysis methods have been used extensively. For example, in ref. [12], the vibration of targeted machine under different operating conditions is reduced by 35% through selecting an optimal carrier frequency, which is optimized by the three-phase pulse-width modulation and non-classic space-vector modulation technique; ref. [13] investigates comprehensively the electromagnetic vibration caused by the side-band harmonic components in the space vector pulse width modulation. The magnetic components are analyzed with the analytical method, and then the amplitude distributions of side-band radial magnetic force components are obtained in different frequency bands.

Other approaches have also been proposed to predict the distribution characteristics of motor noise by finite element (FE) method in the second one. For example, a numerical analysis process for estimating the radiation electromagnetic noise of PMSM is described in ref. [14], the proposed method is verified by experiments in evaluating structural and acoustic responses of the targeted prototype, and which performs a superior precision. Another example such as ref. [15] establishes a multi-physics simulation model to predict the electromagnetic vibration and noise of the motor, and the accuracy of the model is verified through experimental tests. However, these few studies are investigated from the analysis of the pulse-width modulation technique for controlling time-current to the multi-physics FE model (FEM) to predict electromagnetic radiation noise. Therefore, the establishment of a joint simulation system is an optimization analysis trend based on the electronic control, electromagnetic design, structural modeling and acoustics calculation. In which, the influencing factors of electromagnetic noise can be considered comprehensively, and the motor structure parameters can also be reasonably optimized [16,17].

In this paper, a multi-physics simulation model capable of electromagnetic noise prediction is established, and the influence of rotor step skewing on electromagnetic noise distribution is analyzed. Firstly, based on the verified motor model, a rotor step skewing model which can affect electromagnetic noise is analyzed, and the spectrum characteristics of the low-order radial magnetic force are investigated. Secondly, the vibration characteristics of the PMSM are determined by the modified structural modal based on modal test. Thirdly, the radial magnetic force is loaded on the stator tooth surface, and then the vibration response analysis of the motor is carried out with the mode superposition method. Finally, the radiation noise of the whole machine is simulated, and the effectiveness of the established model is verified in predicting and evaluating electromagnetic noise by conducting a motor radiation noise experiment.

2 Structural modeling of PMSM

A PMSM is mainly composed of rotor core, permanent magnets, stator core, windings, housing, anterior and rear end cover, and rotor shaft. In the FE modeling of the motor, the real contact condition between every part of the motor assembly should be considered, and the FE grid of the critical structure should be carefully meshed [18]. The end cover is connected with the machine body through a rigid element, and the contact condition between windings and stator, stator and housing are determined by node coupling. Radial magnetic force is the excitation source of electromagnetic noise, which acts on the tooth surface of stator in air gap, makes the motor vibrate and then radiates noise to the surrounding air [19]. Since the rotor core that is not in contact with the stator and housing directly, so it can be equivalent modeling to a mass block loaded uniformly on the rotor shaft surface when the rotor has a stable electromagnetic torque under steady condition. Therefore, in the structural FE modeling, the rotor core and permanent magnets are simplified as a mass point loaded onto the rotor shaft surface. And the FEM of the whole machine is shown in Figure 1.

Step skewing of rotor magnets can effectively weaken the stator tooth harmonics, and reduce the torque ripple to improve the stability of the motor output torque. Here, in this research, the influence of skewing angle on electromagnetic noise was studied by comparing the characteristics of radial magnetic force with and without step skewing. The structure of step skewed rotor is given in Figure 2.

The study diagram on vibration and noise prediction of PMSM is shown in Figure 3. It is a multi-physics modeling process that consists of electromagnetic analysis, modal analysis, frequency-response analysis and acoustic analysis.

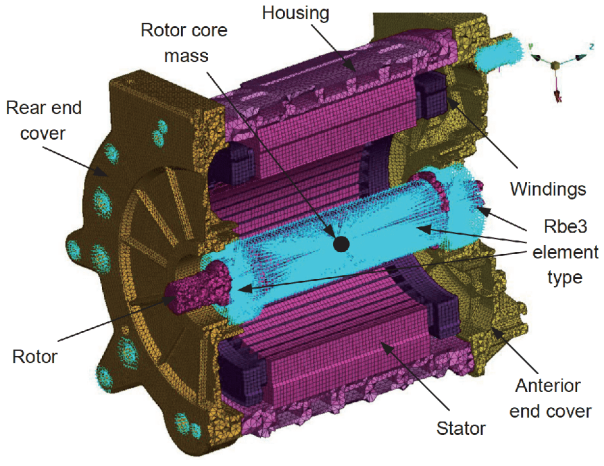

Figure 1 (Color online) FEM of the whole machine.

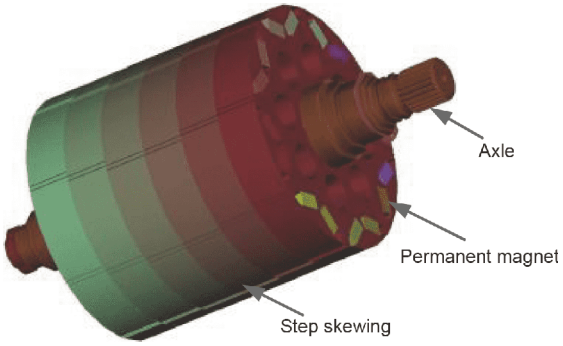

Figure 2 (Color online) Structure of the step skewed rotor.

Among them, the structural modal analysis and acoustic analysis need to be verified by corresponding tests [20]. In the electromagnetic analysis of PMSM with rotor step skewing, the electromagnetic characteristics are different in each air gap section since every skewed rotor has different skewing angle circumferentially. In order to evaluate the vibration characteristics of the PMSM with different skewing angle from the view of the whole machine, a comparative analysis of the noise simulation results is conducted based on a validated structural model.

3 Electromagnetic analysis

3.1 Magnetic flux distribution

In order to obtain the excitation source of electromagnetic vibration, the radial magnetic force of the PMSM is obtained by numerical calculation in the two-dimensional transient magnetic field [21], and the spectrum characteristics of the magnetic force are analyzed [22,23]. The main design parameters of PMSM are given in Table 1.

The selected motor is an interior PMSM. The permanent magnet material is 35UH_80C with relative magnetic permeability of 1.03 and conductivity of 635000 S/m. The motor is powered by a sinusoidal wave current with a fundamental frequency of 265.33 Hz. The magnetic flux distribution is illustrated in Figure 4 under steady-state load at rated speed.

In the air gap, the magnetic flux lines are densely distributed along the circumferential direction and have an obvious periodicity, which can be observed from Figure 5. In the circumferential space, the uneven distribution of magnetic flux lines is the source of electromagnetic vibration and noise.

3.2 Magnetic force calculation

3.2.1 Radial magnetic force at different circumferential positions

In the air gap, the radial force density will vary with time-space because of the magnetic flux density with periodic distribution. The amplitude of radial force density is constantly changing at different times and positions, and the uneven distribution of radial magnetic force will lead to electromagnetic noise. The time history of calculating radial force density in the air gap is

$$f_r(t) = \frac{B_r^2(t)}{2\mu_0}, \tag{1}$$

where $f_r(t)$ is the radial force density, $B_r(t)$ is the radial flux density, and μ_0 is the vacuum permeability.

The spectral distribution of radial force density at different positions is shown in Figure 6. The "distance" shown in Figure 6 refers to the circumferential distance relative to the position where the main magnetic axis coincides between the stator and the rotor at the given time. In this figure, the

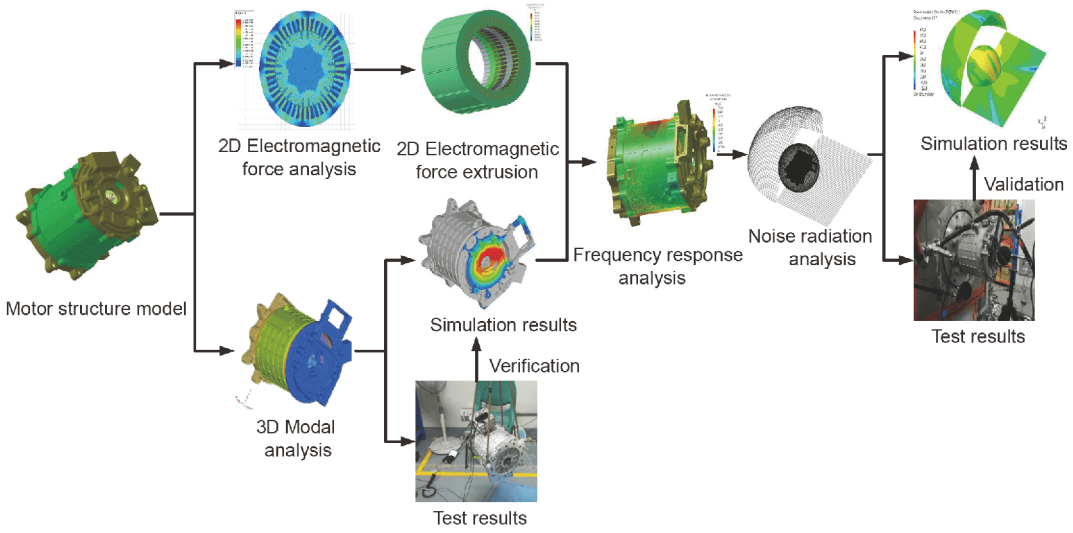

Figure 3 (Color online) The study diagram on vibration and noise prediction of PMSM.

Table 1 Main design characteristic parameters of the PMSM

Parameters	Value
Phases/Poles/Slots	3/8/48
Air gap length	0.602 mm
Opening width	2 mm
Rated speed	3980 r/min
Current amplitude	268 A
Current angle	39.2°
Stator outer diameter	220 mm
Stator inner diameter	143.2 mm
Rotor inner diameter	48 mm
Axial length of rotor	148.8 mm
Skewing angle	2.5°

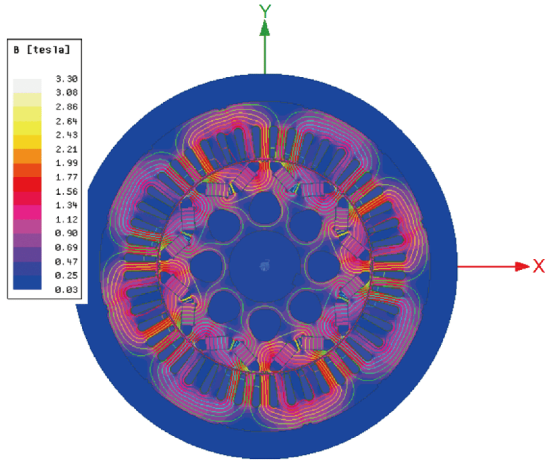

Figure 4 (Color online) Flux distribution load at rated speed.

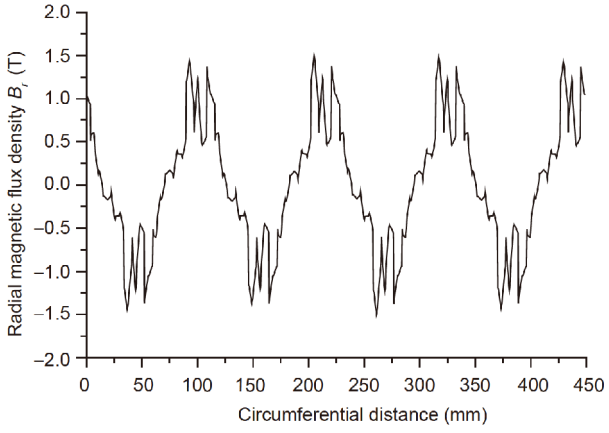

Figure 5 The circumferential distribution of the radial flux density in the air gap.

distribution characteristics of radial force density in different circumferential positions are presented by 4 simulation curves, and the results show that the frequency-domain distribution of radial magnetic force density is similar at different circumferential positions, and the radial force amplitude mainly focuses below 4000 Hz. However, the

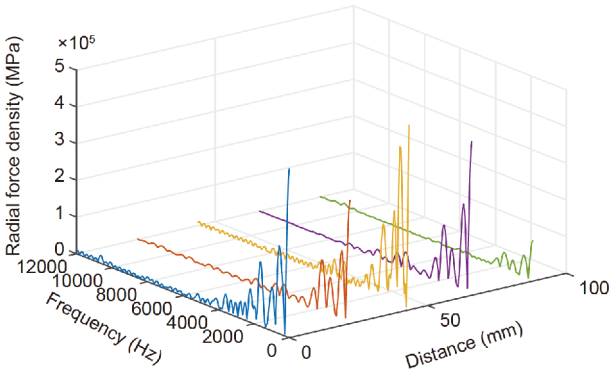

Figure 6 (Color online) Spectral distribution of radial magnetic forces at different positions along the circumference.

amplitude is distinctly different and has a 4 (pole pairs) complete distribution periods in the entire circumference.

By integrating and summing the radial force density in the entire circumference, the radial magnetic force of unit axial distance F_n can be calculated, and the spectrum of radial magnetic force is shown in Figure 7. When the frequency of radial magnetic force acting on the motor is approaching closer to the natural frequency of the motor, the resonance phenomenon will appear and the electromagnetic noise are to be maximized at any of its resonant frequencies.

3.2.2 *Radial magnetic force at different skewing angle*

In the electromagnetic design of PMSM, the skewing angle of the skewed rotor refers to the magnetic axis angle between the rotor *d*-axis and the stator *A*-phase when the motor is working, and its two-dimensional cross-section is shown in Figure 8. The rotor is segmented equidistantly in the axial direction and each stepped rotor has been designed to have a different skewing angle. This structure layout is similar to the effect of the skewed stator slot, which can effectively weaken the tooth harmonics and improve the torque ripple of the PMSM.

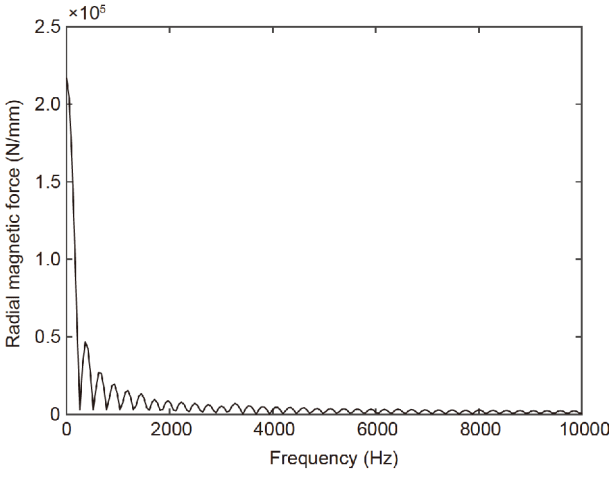

Figure 7 Spectrum of radial magnetic force.

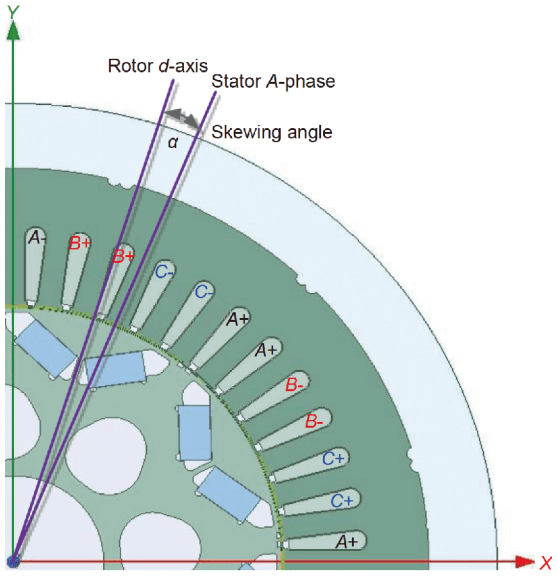

Figure 8 (Color online) Two-dimensional cross-section of the skewed rotor.

The spectrum of radial force density with different skewing angle is given in Figure 9. It is show that the larger the skewing angle, the greater the amplitude of radial force density. And it also can be seen that the frequency at the peak of radial magnetic density is mainly located near the even multiple fundamental frequency.

4 Modal analysis

In the numerical solution and analysis, the FEM of the stator core is constructed according to the geometric dimensions and material properties. The stator core is laminated by silicon steel sheets and shows different properties in cross section and axial direction, so the material properties of the stator core are three-dimensional orthogonal and the elastic properties that are symmetric to three mutually perpendicular

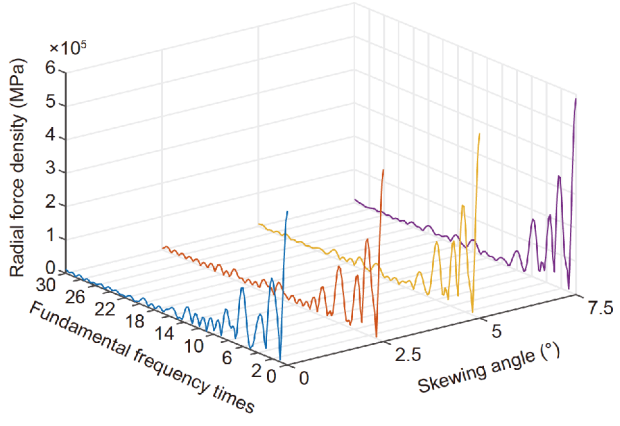

Figure 9 (Color online) Spectrum of radial force density with different skewing angle.

planes are identical. The constitutive relation of stress-strain is represented by elastic modulus as follows:

$$\begin{Bmatrix}\sigma_x\\ \sigma_y\\ \sigma_z\\ \tau_{xy}\\ \tau_{yz}\\ \tau_{zx}\end{Bmatrix} = \mathbf{G}\left[\begin{Bmatrix}\varepsilon_x\\ \varepsilon_y\\ \varepsilon_z\\ \gamma_{xy}\\ \gamma_{yz}\\ \gamma_{zx}\end{Bmatrix} - (T-T_{\text{ref}})\begin{Bmatrix}A_1\\ A_2\\ A_3\\ A_4\\ A_5\\ A_6\end{Bmatrix}\right], \tag{2}$$

where σ, τ, ε and γ are the tensors of normal stress, shear stress, normal strain and shear strain, respectively. T is the structure temperature, T_{ref} is the reference temperature, A is the coefficient of thermal expansion. **G** is the stiffness matrix and it can be represented as

$$\mathbf{G} = \begin{Bmatrix} G_{11} & G_{12} & G_{13} & 0 & 0 & 0\\ G_{12} & G_{22} & G_{23} & 0 & 0 & 0\\ G_{13} & G_{23} & G_{33} & 0 & 0 & 0\\ 0 & 0 & 0 & G_{44} & 0 & 0\\ 0 & 0 & 0 & 0 & G_{55} & 0\\ 0 & 0 & 0 & 0 & 0 & G_{66}\end{Bmatrix}, \tag{3}$$

the stiffness matrix **G** can be expressed as the elastic modulus:

$$\begin{aligned} G_{11} &= \frac{1-\mu_{yz}\mu_{zy}}{E_yE_z\Delta}, G_{44} = G_{yz},\\ G_{22} &= \frac{1-\mu_{xz}\mu_{zx}}{E_xE_z\Delta}, G_{55} = G_{xz},\\ G_{33} &= \frac{1-\mu_{xy}\mu_{yx}}{E_xE_y\Delta}, G_{66} = G_{xy},\\ G_{12} &= \frac{\mu_{xy}+\mu_{xz}\mu_{zy}}{E_xE_z\Delta} = \frac{\mu_{yx}+\mu_{zx}\mu_{yz}}{E_yE_z\Delta},\\ G_{13} &= \frac{\mu_{xz}+\mu_{xy}\mu_{yz}}{E_xE_y\Delta},\\ G_{23} &= \frac{\mu_{zy}+\mu_{xy}\mu_{zx}}{E_xE_z\Delta} = \frac{\mu_{xy}+\mu_{yx}\mu_{xz}}{E_xE_y\Delta}, \end{aligned} \tag{4}$$

where the mathematical expression of Δ is defined in the eq. (5), E is Young's modulus, μ is the shear modulus. The relationship between E and μ in different directions is shown in eq. (6).

$$\Delta = \frac{1}{E_xE_yE_z}\begin{vmatrix} 1 & -\mu_{yz} & -\mu_{zx}\\ -\mu_{xy} & 1 & -\mu_{zy}\\ -\mu_{xz} & -\mu_{yz} & 1\end{vmatrix}, \tag{5}$$

$$\begin{aligned} \mu_{yz} &= \mu_{xy}\frac{E_y}{E_x},\\ \mu_{zx} &= \mu_{xz}\frac{E_z}{E_x},\\ \mu_{zy} &= \mu_{yz}\frac{E_z}{E_y}. \end{aligned} \tag{6}$$

Hence, the contact relationship between stator core and

windings is established in a way of node coupling. Since the stator core is laminated by silicon steel sheets and the windings consist of copper wires, so it is impractical to model every steel sheet and copper wire, then the stator core and windings are modeled respectively into an entire solid in the structural FEM, as shown in Figure 10. The material parameters of stator core and windings are not determined until repetitively modifying the simulation model for a number of times, as shown in Table 2.

When the effect of temperature on material properties is overlooked, the stiffness matrices $\mathbf{G}_{\text{core}}$ and $\mathbf{G}_{\text{winding}}$ are obtained respectively based on the validated parameters in the numerical solution.

$$\mathbf{G}_{\text{core}} = \begin{Bmatrix} 168.6 & 76.3 & 85.7 & 0 & 0 & 0 \\ 76.3 & 168.6 & 85.7 & 0 & 0 & 0 \\ 85.7 & 85.7 & 200 & 0 & 0 & 0 \\ 0 & 0 & 0 & 6.5 & 0 & 0 \\ 0 & 0 & 0 & 0 & 6.5 & 0 \\ 0 & 0 & 0 & 0 & 0 & 30 \end{Bmatrix} \text{GPa}, \tag{7}$$

$$\mathbf{G}_{\text{winding}} = \begin{Bmatrix} 12.3 & 4.6 & 3.0 & 0 & 0 & 0 \\ 4.6 & 12.3 & 3.0 & 0 & 0 & 0 \\ 3.0 & 3.0 & 7.1 & 0 & 0 & 0 \\ 0 & 0 & 0 & 3.5 & 0 & 0 \\ 0 & 0 & 0 & 0 & 3.5 & 0 \\ 0 & 0 & 0 & 0 & 0 & 4.1 \end{Bmatrix} \text{GPa}. \tag{8}$$

In the hammering modal test, the acceleration sensors are attached to the outer surface of the stator core, so that the modal frequency and modal shape are obtained based on the vibration characteristics of the stator structure. In order to evaluate the modal test result clearly, the local modal caused by the windings will be eliminated in the numerical calculation. Then the first five order measured result is achieved according to the spatial modal shape of the stator, which is listed in Table 3.

The structural FEM that can accurately behave the vibration characteristics of the stator is constructed based on the modified simulation parameters, which is in good agreement with the experimental results in both the mode shape and natural frequency. The average relative error of the first five orders of the modal analysis is 4.3%. However, since some non-linear factors are neglected in the process of FE calculation, such as the influence of temperature on material properties, the simplification of contact relationship between windings and stator core, and the dissatisfactory accuracy of material parameters, the error will be relatively larger.

Figure 10 (Color online) Structural FEM of stator core and windings.

Table 2 Material parameters of stator core and windings

Parameters	Stator core	Windings
Material	Silicon steel	Copper wire
Young's modulus	E_x=E_y=120 GPa, E_z=140 GPa	E_x=E_y=10 GPa, E_z=6 GPa
Shear modulus	μ_{yz}=μ_{zx}=6.5 GPa, μ_{xy}=30 GPa	μ_{yz}=μ_{zx}=3.5 GPa, μ_{xy}=4.1 GPa
Density	9950 kg m^{-3}	6500 kg m^{-3}
Poisson ratio	0.3	0.3

Table 3 Comparison between simulation and test results

Modal order	Modal shapes	Simulation results (Hz)	Test results (Hz)	Relative error
1		742.9	702.6	5.7%
2		969.3	959.7	1.0%
3		2013.3	1934.2	4.1%
4		3147.8	3249.5	3.2%
5		6192.4	5770.3	7.4%

Finally, the vibration characteristics of the whole machine are revised based on the modified stator structure, and the modal test of the stator and whole machine is shown in Figure 11. The frequency response curve of the whole machine can be obtained by analyzing and processing the acquired modal data, which is shown in Figure 12, in which, the frequency at the peak corresponds to the natural frequency of the motor assembly at each order. The comparisons of the experimental and simulation results of the first three prominent orders are shown in Figure 13.

5 Noise prediction and test verification

5.1 Noise prediction

The electromagnetic vibration of motor belongs to the forced one under the action of radial magnetic force. Therefore, when the frequency of the radial magnetic force is approaching closer to the natural frequency of the whole ma-

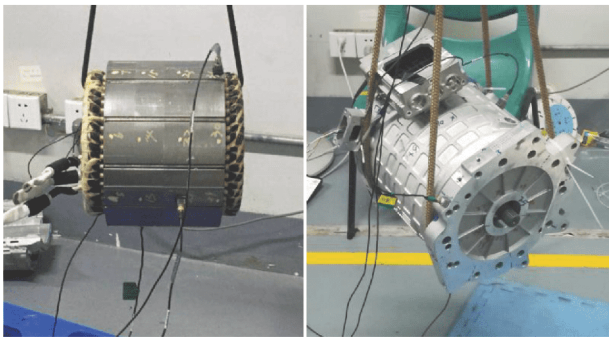

Figure 11 (Color online) Modal test. (a) Stator core and windings; (b) motor assembly.

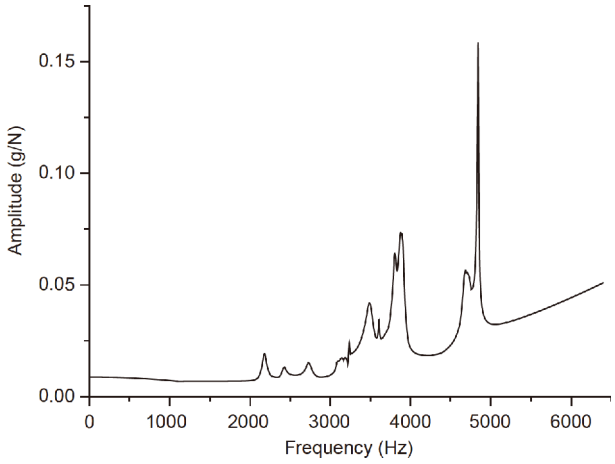

Figure 12 (Color online) Frequency response curve of the motor assembly.

chine, larger noise will be radiated [24]. The motor studied in this paper is a PMSM with poles/slots of 8/48 and a rated/peak speed of 3980/9000 r/min. The acoustic FEM is used to calculate the radiation noise of the PMSM. The sound pressure level (SPL) distribution near the first-order modal frequency is shown in Figure 14. At this point, the maximum SPL is 62.5 dB, and the spectrum of SPL is shown in Figure 15, which is obtained from the field point at the radial side of the motor.

In Figure 15, the frequency-domain distribution of the SPL is calculated by the FEM with or without skewing. It can be seen that the fluctuation trend of two curves is consistent in the frequency range. There is a peak in the natural frequency region of the motor structure. However, on the overall SPL, the noise amplitude of the FEM with skewing of 106 dB is higher than the one without skewing of 85 dB. This is because, in the step skewing FEM, the main flux axis determined by the permanent magnets has a skewing angle with the one determined by the windings, and then more harmonic magnetic potential would be generated. When the motor is working, the low-order radial magnetic force that is caused by the interaction between the permanent magnetic field and the armature field has a significant effect on the electromagnetic noise [25].

5.2 Test Verification

The test device composed by PMSM, electric machine controller, frequency conversion cabinet, high-voltage wiring harness, signal wiring harness and vibration and noise acquisition equipment (including digital acquisition system, microphone and acceleration sensor, etc.). And the test device diagram is described in Figure 16.

The device needs to be debugged before it can be formally tested. During the testing process, the microphone is installed near the axial end cover and radial side of the motor, and the digital acquisition equipment is connected. Then the noise of the PMSM is measured according to the working condition shown in Figure 17, and the bench test is shown in Figure 18.

The test results of the PMSM under the whole machine conditions are shown in Figure 19. The maximum SPL of the tested motor is 106 dB, which occurs around 7400 r/min.

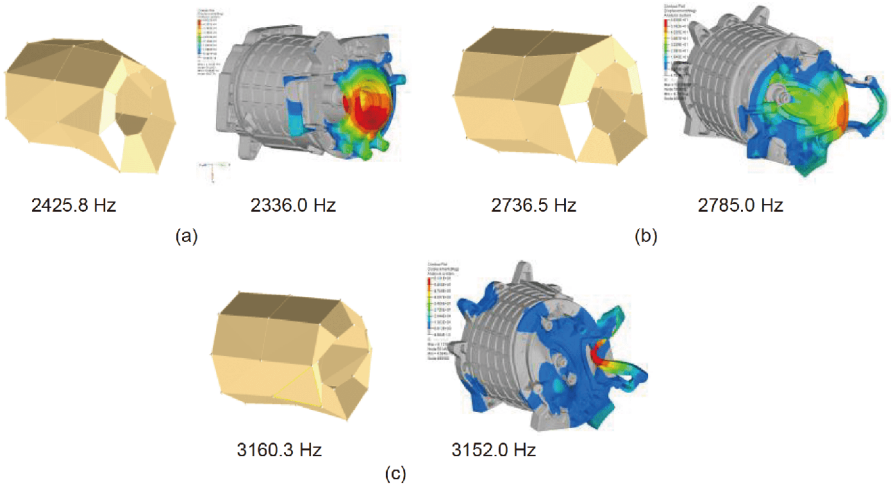

Figure 13 (Color online) Comparisons of the experimental and simulation results of the machine.

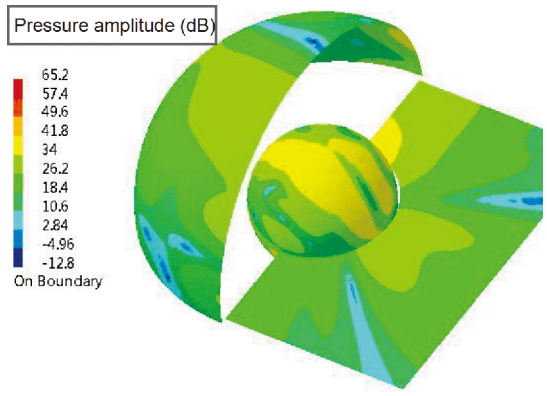

Figure 14 (Color online) Sound pressure distribution near the first-order modal frequency.

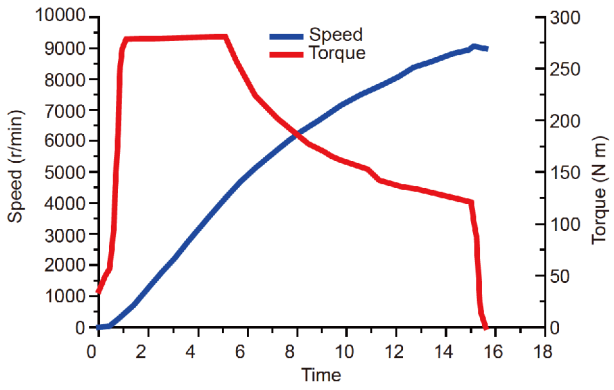

Figure 17 (Color online) NVH bench test conditions of the PMSM.

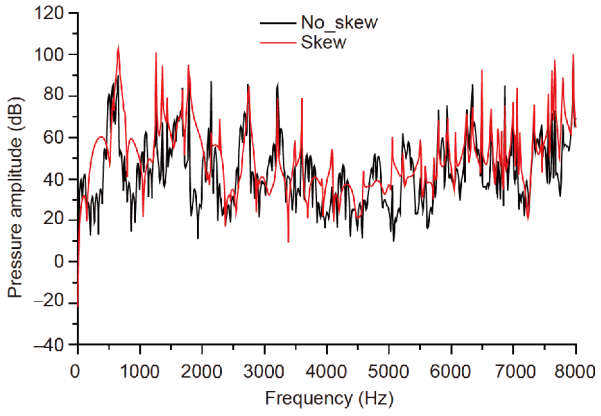

Figure 15 (Color online) Spectrum of SPL of the PMSM.

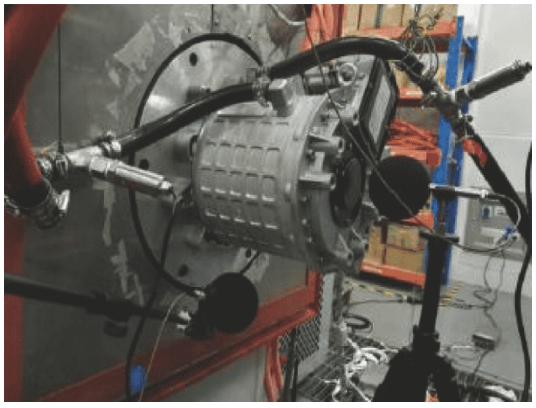

Figure 18 (Color online) NVH bench test of the PMSM.

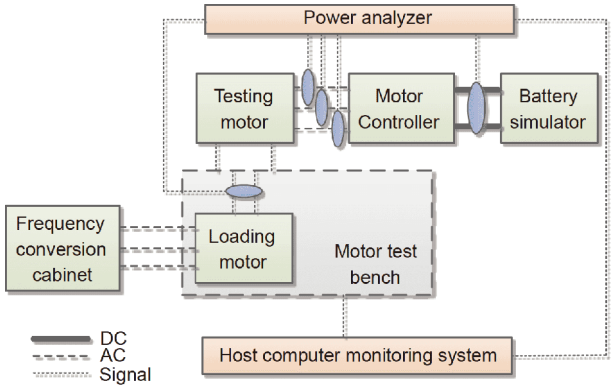

Figure 16 (Color online) Test device diagram of the PMSM.

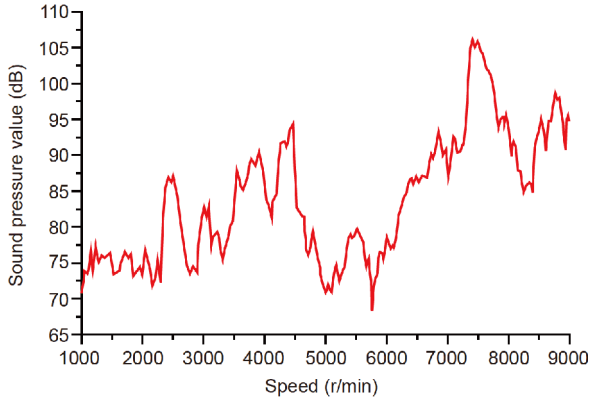

Figure 19 (Color online) Results of noise test under the whole machine conditions.

And at a rated speed of 3980 r/min, the SPL is 87 dB, which is close to the simulated SPL of 85 dB without the step skewing. However, there are some obvious deviations, on the whole, between the calculated and measured results.

In the multi-physics simulation model, some reasons can be responsible for the deviations. For example, the structural FEM and contact relationship of the PMSM are equivalently simplified and cannot fully behave the structural pattern of the motor. Moreover, in the simulation calculation process, the motor is calculated in an ideal no-load state, while some friction torques need to be overcome before the motor startup in the test process [26]. In addition, the electromagnetic vibration and noise are dominantly attributed to the radial magnetic force in this prediction model, while the actual motor noise is not only from electromagnetic noise, but also from the mechanical noise caused by the rotor imbalance and torque ripple of the PMSM [27–29].

However, by comparing the calculated and tested results,

the multi-physics simulation model proposed in this work is effective for evaluating the electromagnetic vibration and noise of PMSM.

5.3 Results and discussion

Based on the simulation and experimental results, in order to weaken the electromagnetic vibration and noise of the PMSM, some measures can be taken from the following aspects in the electromagnetic design of driving motor.

(1) The natural frequency of the motor structure has a significant effect on the electromagnetic noise. In order to decrease the electromagnetic noise level of the motor, the frequency of radial magnetic force should be kept away from the natural frequency of the PMSM as far as possible in the design of the driving motor, so as to avoid generating electromagnetic resonance within the working speed range.

(2) The rotor skewing angle has an obviously impact on the magnetic force amplitude. Under the premise of considering the motor torque ripple, a smaller skewing angle should be considered, which can weaken the harmonic magnetic potential generated in the stator and rotor magnetic field and reduce the amplitude of low-order radial magnetic force, and then the electromagnetic noise can be weakened.

(3) Harmonic magnetic potential can affect the electromagnetic vibration and noise. The stator and rotor slot should be rationally designed and the windings arrangement should be optimized, to reduce the stator harmonic potential and make the rotor magnetic potential close to the sinusoidal wave, thus reducing the electromagnetic vibration noise of the PMSM.

(4) In the process of modeling, it is necessary to consider the actual contact relationship and constraint conditions between various parts of the motor assembly. To obtain a more accurate prediction results, the motor structure should be reasonably simplified and the FEM should be constantly modified according to the test results, and then a multi-physical field simulation model can be constructed to evaluate and analyze the electromagnetic vibration and noise of the PMSM.

6 Conclusions

In the present study, a multi-physics simulation model capable of predicting electromagnetic noise is established. Based on the validated prediction model, a rotor step skewing model is proposed. Then the spectrum of low-order radial magnetic force which has a great impact on motor noise is investigated. Finally, the influence of the skewing angle on the electromagnetic noise is analyzed and the following conclusions can be drawn.

(1) By comparing the simulation results with the experimental results, the distribution characteristics of the motor electromagnetic noises can be theoretically predicted and rationally explained by the established multi-physics simulation model. It is effective and feasible to evaluate the electromagnetic vibration and noise of the PMSM. The results show that the SPL of the tested machine without skewing is 87 dB, which is close to the predicted SPL of 85 dB. The difference between the two results is mainly due to the reasonable equivalence and assumption of the structure and contact relationship of the motor in the multi-physics simulation model, it ignores the frictional torque that needs to be overcome in the motor startup and the mechanical noise caused by the torque ripple and rotor imbalance.

(2) Based on the feasibility of the validated prediction model, the influence of skewing angle on the electromagnetic noise is evaluated. The spectral variation of electromagnetic noise is consistent between the motor with and without rotor step skewing in the frequency range, but the SPL of the motor with rotor step skewing is higher than that of the motor without rotor step skewing. This is because more harmonic magnetic potentials would be generated when the main flux axis determined by the permanent magnets is at an angle to the main flux axis determined by the windings, and the low-order radial magnetic force caused by these harmonic magnetic potentials would has a significant influence on the motor noises.

(3) The spectral analysis of the radial force density with different skewing angles shows that the frequency at the peak of the radial force density is similar at different positions along the circumference, and the frequency at the peak is mainly located below 4000 Hz. The spectrum of the radial force density is different under different skewing angles. The larger the skewing angle, the larger the radial force density. And the frequency at the peak of the radial force density is mostly distributed near the even multiple fundamental frequency.

This work was supported by the National Natural Science Foundation of China (Grant No. 51675324).

1 Ma C G, Zuo S G. Black-box method of identification and diagnosis of abnormal noise sources of permanent magnet synchronous machines for electric vehicles. IEEE Trans Ind Electron, 2014, 61: 5538–5549
2 Zou J B, Lan H, Xu Y X, et al. Analysis of global and local force harmonics and their effects on vibration in permanent magnet synchronous machines. IEEE Trans Energy Convers, 2017, 32: 1523–1532
3 Wu S, Zuo S G, Wu X. Numerical prediction and analysis of electromagnetic vibration and noise of claw pole alternator. J Acoust Soc Am, 2016, 139: 2104
4 Fang Y, Zhang T. Vibroacoustic characterization of a permanent magnet synchronous motor powertrain for electric vehicles. IEEE Trans Energy Convers, 2018, 33: 272–280
5 Min S G, Sarlioglu B. Modeling and investigation on electromagnetic noise in PM motors with single- and double-layer concentrated

winding for EV and HEV application. IEEE Trans Transp Electrific, 2018, 4: 292–302
6 Jung J W, Lee S H, Lee G H, et al. Reduction design of vibration and noise in IPMSM type integrated starter and generator for HEV. IEEE Trans Magn, 2010, 46: 2454–2457
7 Ma C, Liu Q, Wang D, et al. A novel black and white box method for diagnosis and reduction of abnormal noise of hub permanent-magnet synchronous motors for electric vehicles. IEEE Trans Ind Electron, 2016, 63: 1153–1167
8 Carraro E, Bianchi N, Zhang S, et al. Design and performance comparison of fractional slot concentrated winding spoke type synchronous motors with different slot-pole combinations. IEEE Trans Ind Appl, 2018, 54: 2276–2284
9 Ryi J, Choi J S. Noise reduction effect of airfoil and small-scale rotor using serration trailing edge in a wind tunnel test. Sci China Tech Sci, 2017, 60: 325–332
10 Liu T, Li J, Cai X, et al. A time-frequency analysis algorithm for ultrasonic waves generating from a debonding defect by using empirical wavelet transform. Appl Acoust, 2018, 131: 16–27
11 Zhu L, Yang Q, Yan R, et al. Magnetoelastic numerical analysis of permanent magnet synchronous motor including magnetostriction effects and harmonics. IEEE Trans Appl Supercond, 2014, 24: 1–4
12 Torregrossa D, Paire D, Peyraut F, et al. Active mitigation of electromagnetic vibration radiated by PMSM in fractional-horsepower drives by optimal choice of the carrier frequency. IEEE Trans Ind Electron, 2011, 59: 1346–1354
13 Liang W, Luk P C K, Fei W. Analytical investigation of sideband electromagnetic vibration in integral-slot PMSM drive with SVPWM technique. IEEE Trans Power Electron, 2016, 32: 4785–4795
14 Torregrossa D, Peyraut F, Fahimi B, et al. Multiphysics finite-element modeling for vibration and acoustic analysis of permanent magnet synchronous machine. IEEE Trans Energy Convers, 2011, 26: 490–500
15 Lin F, Zuo S G, Deng W Z, et al. Reduction of vibration and acoustic noise in permanent magnet synchronous motor by optimizing magnetic forces. J Sound Vib, 2018, 429: 193–205
16 Zhang G, Hua W, Cheng M. Nonlinear magnetic network models for flux-switching permanent magnet machines. Sci China Tech Sci, 2016, 59: 494–505
17 Wu J, Yan S, Li J, et al. Mechanism reliability of bistable compliant mechanisms considering degradation and uncertainties: Modeling and evaluation method. Appl Math Model, 2016, 40: 10377–10388
18 Yu S B, Tang R. Electromagnetic and mechanical characterizations of noise and vibration in permanent magnet synchronous machines. IEEE Trans Magn, 2006, 42: 1335–1338
19 Zuo S, Lin F, Wu X. Noise analysis, calculation, and reduction of external rotor permanent-magnet synchronous motor. IEEE Trans Ind Electron, 2015, 62: 6204–6212
20 Liu X T, Rao S S. Vibration analysis in the presence of uncertainties using universal grey system theory. J Vib Acoust, 2018, 140: 031009
21 Islam M S, Islam R, Sebastian T. Noise and vibration characteristics of permanent-magnet synchronous motors using electromagnetic and structural analyses. IEEE Trans Ind Appl, 2014, 50: 3214–3222
22 Yang X B, Liu X T, Tong J C, et al. Research on load spectrum construction of bench test based on automotive proving ground. J Test Eval, 2018, 46: 20170201
23 Wang M L, Liu X T, Wang X L, et al. Research on load-spectrum construction of automobile key parts based on monte carlo sampling. J Test Eval, 2018, 46: 20160296
24 Boutora Y, Takorabet N, Ibtiouen R. Analytical model on real geometries of magnet bars of surface permanent magnet slotless machine. PIER B, 2016, 66: 31–47
25 He G, Huang Z, Qin R, et al. Numerical prediction of electromagnetic vibration and noise of permanent-magnet direct current commutator motors with rotor eccentricities and glue effects. IEEE Trans Magn, 2012, 48: 1924–1931
26 Dong Q C, Qi H Z, Liu X T, et al. Calibration and optimization of an electric vehicle powertrain system. J Chin Inst Eng, 2018, 41: 539–546
27 Qiu Y, Rao S S. A fuzzy approach for the analysis of unbalanced nonlinear rotor systems. J Sound Vib, 2005, 284: 299–323
28 Wang W, Wang H, Karimi H R. Study on the characteristics of electromagnetic noise of axial flux permanent magnet synchronous motor. Abstract Appl Anal, 2014, 2014: 1–8
29 Besnerais J L. Vibroacoustic analysis of radial and tangential air-gap magnetic forces in permanent magnet synchronous machines. IEEE Trans Magn, 2015, 51: 8105609